ISSN: 0975-8585

Research Journal of Pharmaceutical, Biological and Chemical Sciences

Synthesis and Catalytic Activity of Vanadia-Doped Iron-Pillared Clays for Cyclohexene Epoxidation.

S Brahimi, S Boudjema, I Rekkab, A Choukchou-Braham*, and R Bachir.

Laboratoire de Catalyse et Synthèse en Chimie Organique, Faculté des sciences, University of Tlemcen 1300, Algeria

ABSTRACT

We prepared the catalysts based on montmorillonite which was obtained from purified Algerian clay (Maghnia, Tlemcen). The montmorillonite was pillared by iron and doped with vanadia at different ratios V/Fe-Mont. The materials prepared were characterized by UV-visible and nitrogen adsorption-desorption at 77 K. The surface acidities of the samples and their structures were also investigated with the gas phase adsorption data of pyridine, using the FT-IR spectroscopic technique. The FT-IR spectra of the samples reflected mainly the structure of Bentonite. The nitrogen adsorption-desorption isotherms of the samples were type IV shaped and showed in general mesoporous structures with pore openings of 4 nm. An infrared study of pyridine adsorption on the samples showed both Lewis and Brønsted sites on their surfaces. Vanadia-doped iron-pillared clay was tested in cyclohexene epoxidation. These materials are good catalysts for liquid phase epoxidation of cyclohexene, when using TBHP as oxidant. The effects of various factors on catalyst reactivity were also studied. The performance and selectivity of the catalysts were enhanced in aprotic/apolar solvents (heptane) when compared to protic/apolar (acetic acid) or aprotic/polar (acetonitrile) solvents. Catalytic activity values of the materials were also calculated.

Keywords: Iron –pillared clay, Vanadia, Intercalation, Epoxidation.

Corresponding author

ISSN: 0975-8585

INTRODUCTION

Various reports in recent years have attracted attention for a new class of microporous and mesoporous solids by intercalating clay, with monocations [1], such as montmorillonite, whose porosity and acidity may be adapted after special treatments [2]. Many researchers have thus expressed interest in clays, which have been modified through pillaring, and their wide range of potential applications in catalytic process [3-11]. Introducing inorganic pillars, in addition to improving clay mineral strength and its stability, increases the microporosity and provides a greater surface area on the solid, thereby facilitating reagents' access to potentially active sites for the catalysis of some reactions [12]. Iron oligomers are some of the most widely used pillaring agents, because iron-pillared clays are cheaper to prepare and would not only have acidic properties but also contain pillars that in themselves would be catalytically active and have redox and magnetic properties [13].

(Cyclo)alkene epoxidation is a key transformation in organic synthesis, both on an academic and industrial scale, for the production of various chemicals. Epoxides form an important group of compounds, obtained by catalytic oxidation, and are strategic intermediates in the chemical industry. They can be converted into alcohols, polyethers and aldehydes, compounds that show widespread applications in the chemical, agrochemical and pharmaceutical industries [14, 15]. Many catalytic systems, based on transition metals, such as Fe and V [16], have been realized using several oxidants, such as oxygen, hydrogen peroxide, and tert-butylhydroperoxide, among others; they were found to be very effective and selective for the epoxidation of a wide range of (cyclo)alkenes, using hydroperoxides as oxidants [17-19].

Among these transition metals, vanadium has a special importance in oxidation chemistry due to its wide range of oxidation states (+2 to +5) in an aqueous solution, and is a well-studied catalyst in selective oxidation [20, 21]. The catalytic activity depends on the physicochemical properties of vanadium active sites [22, 23]. Cyclohexene epoxidation has been widely investigated using several metal catalysts under homogeneous and heterogeneous conditions [24-28].

It has been shown [29] that epoxidation of cyclohexene, using aqueous hydrogen peroxide (30 %, v/v) over iron–cerium oxide, leads to a higher cyclohexene conversion (~ 99 mol %); epoxide selectivity rates (98 %) were observed when 5%Fe/CeO_2 was employed as the catalyst. In addition, it is well-known that vanadium is an efficient catalyst in various organic reactions [30]. Recently many works have investigated its catalytic activity either as homogeneous oxovanadium complexes or as supported catalysts in epoxidation reactions [31-33]. Several mechanisms have been proposed for the oxidation reactions. On the one hand, the Mars and van Krevelen mechanism, proposed by Corma et al., states that the oxidation reactions are managed by a number of Lewis acid, Lewis basic and redox centers [34]. On the other hand, Busch et al. suggest another mechanism involving Lewis acids for the epoxidation of olefins [35].

The activation energy is the minimum amount of energy required to initiate a reaction. It is one of the important indicators for appraising a reaction. The chemical reaction rate is closely related to the value of the activation energy. The lower the activation energy, the faster the reaction rate is. The activation energy of the catalyst used is calculated and compared with the reported values of similar reactions [36-42].

In this work, we studied the catalytic performance of vanadia supported on iron-pillared clay prepared from a natural Algerian Bentonite, in cyclohexene epoxidation. The main products of the reaction were the epoxide, one, enone, ol, enol, diol. The effects of various reaction parameters such as the catalyst weight, the reaction temperature and the solvent effects were investigated. The catalytic materials were characterized by Diffuse-reflectance UV-vis spectroscopy, surface acidity followed by FT-IR spectroscopy and nitrogen adsorption-desorption isotherms, in order to correlate their physico-chemical features to the catalytic performances.

EXPERIMENTAL

Materials

The starting clay used was a Bentonite from Maghnia; it is a natural clay mineral with a (0 0 1) spacing of 10 Å. It belongs to the montmorillonite family. The clays are aluminosilicates of 2/1 type with the theoretical

formula $M_xSi_4O_{10}(Al_{2-x}R_x)(OH)_2{\cdot}nH_2O$, with M and R corresponding, respectively, to monovalent and divalent cations. The number of water molecules (*n*) and the extent of substitution (*x*) can vary from one compound to the other; cation M can also correspond in some cases to divalent or trivalent cations. Before intercalation, the bentonite was purified. So, 10 g of natural clay were ground, sieved to 100 µm and dried at 80 °C. They were dispersed into 1 L of distilled water for 2 h and allowed to settle for 16 h. The first 450 mL of the suspension were separated from the bottom and dried at 80 °C. They were then dispersed 3 times into 1 L of NaCl (1.5 M) for 4 h and washed with distilled water.

Intercalation procedure

A 0.6 wt.% colloidal suspension of clay was first prepared by dispersing the purified Bentonite into water under stirring. In parallel, $FeCl_3.6H_2O$ was added to NaOH. The solution was characterized by a Fe/OH molar ratio equal to 2.

In order to avoid precipitation of Fe species, the pH was kept constant at 1.7. The resulting solution was aged for 4 h and stirred at room temperature. It was observed that ageing times ≤ 12 h did not have any practical influence on the physical properties of the pillared materials. The pillaring solution was then slowly added to the suspension of Bentonite in deionized water. The relative volume of the two solutions was chosen to have a final iron to clay ratio equal to 30 mmol g^{-1}. The mixture was stirred and allowed to react. Finally, the solid was washed by vacuum filtration with deionized water until no chloride remained (test $AgNO_3$). The aim of this operation was to remove excess chloride ions which could prevent the diffusion of polyoxocations within the interlayer space [43]. The solid was air dried and the resulting product was calcined at 500 °C for 5 h [44]. The final product is referred to as Fe-Mont herein.

Vanadia impregnation

Vanadia-loaded Fe-Mont, containing 3, 6 and 9 wt.% vanadia, were prepared through the wet impregnation of the Fe-Mont support, using the 0.1 molar aqueous solution of NH_4VO_3 (99 %, Aldrich). For exchange with vanadium, 50 mL of ammonium metavanadate were dissolved into 50 mL of oxalic acid. Finally, all the samples were dried at 80 °C for 24 h and calcined at 550 °C for 5 h. The samples were labeled as Xwt.%V/Fe-Mont, where X refers to the vanadia loading.

Characterization methods

Diffuse-reflectance UV-visible spectra (200-800 nm) of these samples were collected upon a Perkin-Elmer Lambda 800 UV/vis spectrophotometer equipped with a diffuse reflectance accessory to collect the diffuse reflected light only. The baseline was recorded using $BaSO_4$ as a reference material.

The specific surface area, pore and micropore volumes of the samples were determined from the N_2 adsorption isotherms at 77 K using a Quantachrome Nova 1000^e instrument. The pore size distribution was calculated by the BJH method from the desorption branch. The surface area and micropore volume were calculated using the t-plot-De Boer method. Prior to physisorption measurements, the samples were outgassed at 250 °C for 3 h, under vacuum.

The FT-IR spectra of the solid samples were recorded using an Agilent Technologies Cary 60 series FT-IR spectrometer, with ATR accessories, and a measuring range of 400–4000 cm^{-1}.

FT-IR measurement of the pyridine adsorbed was carried out on a NEXUS- Nicolet spectrometer at a 4 cm^{-1} resolution and a 400–4000 cm^{-1} scanning range. The spectrometer was equipped with an MCT detector cooled by liquid nitrogen. Approximately 18-20 mg of the catalyst sample were pressed into a self-supported wafer of approximately 2 cm in diameter, followed by evacuation at 623 K for 4 h, after being cooled down to 293 K. A known amount of pyridine was then introduced into the wafer at room temperature and degassed at 423 K for 15 min, to remove the physisorbed fraction. Finally the pyridine adsorption was followed by evacuation for 15 min at 323, 373, 423 and 473 K. The IR spectrum thus obtained was used to calculate the amount of acid sites on the sample by measuring the areas of pyridine adsorption peaks.

ISSN: 0975-8585

Catalytic experiments

The catalytic epoxidation of cyclohexene with tertiobutylhydroperoxyde TBHP (Aldrich 70 wt. % in H_2O) as an oxidant was carried out in a two-neck glass round-bottom flask equipped with a magnetic stirrer and a reflux condenser, or in an autoclave at atmospheric pressure. First, TBHP was stirred with n-heptane as solvent, in order to perform a transfer from water phase to organic phase. Typically, 25 mL of n-heptane and 38.45 mmol (5.5 mL) of oxidant (TBHP) were mixed in a closed Erlenmeyer flask and magnetically stirred for 24 h. The organic phase was then separated from the aqueous phase. To control the phase transfer, the concentration of the remaining TBHP in the aqueous phase was regularly determined by iodometric titration.

Less than 10 % of the initial TBHP remained in the aqueous phase, then 29 mmol (3 mL) of cyclohexene was added to the TBHP-heptane mixture which was afterwards heated to 70 °C, under vigorous stirring. At time zero, a quantity of 100 mg of the catalyst was added to the previous mixture. The reaction products were examined by gas chromatography (GC), using a SCHIMADZU GC 14-B equipped with the capillary column "Agile HP-FFAP" and a flame ionization detector (FID). Before GC analysis, the remaining TBHP was decomposed by introducing an excess of triphenylphosphine (Aldrich). On the other hand, in order to control the remaining TBHP, an iodometric titration was performed at the end of the reaction (after 6 h) by analyzing the organic phase.

$$Conversion\ (\%) = 100 \times \frac{[C_6H_{10}]_0 - [C_6H_{10}]_t}{[C_6H_{10}]_0}$$

$$Selectivity\ (\%) = 100 \times \frac{moles\ of\ individual\ product}{moles\ of\ total\ products}$$

RESULTS AND DISCUSSION

Characterization

UV-vis diffuse reflectance spectroscopy (UV-vis-DRS)

UV–vis-diffuse reflectance spectroscopy (UV–vis-DRS) is a technique suitable for studying the coordination environment of metal ions in constrained environments, such as in zeolites and clay materials [45, 46]. Fig. 1 and Fig. 2 illustrate the UV–vis-DRS spectra of the samples. Na-Mont displays a characteristic broad band centered at about 250 nm, which is assigned to the ($Fe^{3+} \leftarrow O^{2-}$, OH^-, or OH_2) charge transfer band for the structural iron present in the octahedral layer of the clay mineral [1, 47].

Figure 1: UV-vis-DRS spectra of iron pillared systems

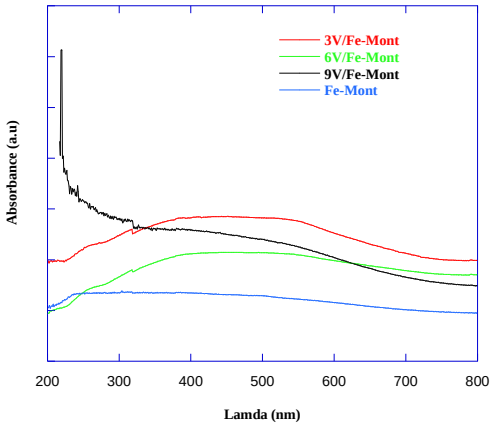

ISSN: 0975-8585

In Fe-Mont, compared to bentonite, a slight increase in the intensity of the shoulders is observed at 500 nm; this is due to the intervalence Fe–O–Fe charge transfer in the chain-type iron-alumina pillars of the clay. In the case of V/Fe-Mont, the spectrum is dominated by two charge-transfer (CT) bands of V^{5+}: one below 300 nm and the other around 350–400 nm. It has been reported that, for oxoanions of V^{5+} ($3\ d^0$), a very strong absorption due to the CT transition between oxygen ligands and the central V atoms is generally observed in the UV–vis region [48, 49]. The values of these electronic CT energies are strongly influenced by the local structure of the V sites and the size of the V domains investigated. In general, isolated tetrahedral monomeric species give rise to CT transitions in a higher-energy (lower wavelength) range than polymeric species. Accordingly, the band observed below 300 nm can be assigned to the low-energy ligand-to-metal charge-transfer (LMCT) transitions (O^{2-} to V^{5+}) associated with the isolated tetrahedral monomeric species, and the band around 350–400 nm to the polymeric vanadia chains [50, 51]. These polymeric species are formed by isolated tetrahedral vanadium species with the formation of V-O-V bridges.

Figure 2: Deconvolution of 6V/Fe-Mont

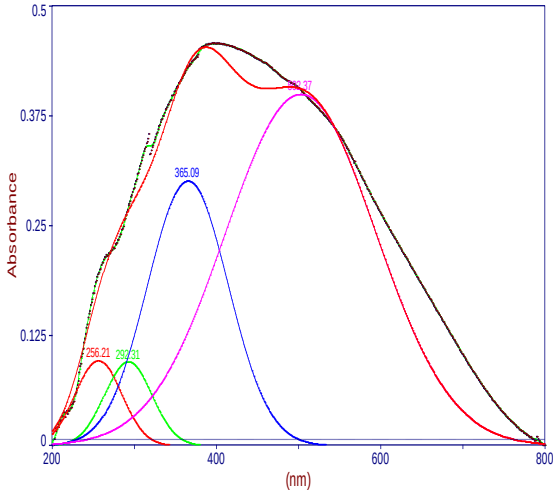

FTIR analysis

FTIR spectroscopy provides complementary evidence for the formation of pillared clay; the FTIR spectra of the samples are illustrated in Fig. 3. The FTIR spectrum of Fe-Mont shows bands at 3630 and 3440 cm^{-1} in the –OH stretching region; these two bands are assigned to the –OH stretching vibration of the structural hydroxyl groups in the clay and the water molecules present in the interlayer, respectively [51-54].

Figure 3: FTIR of materials

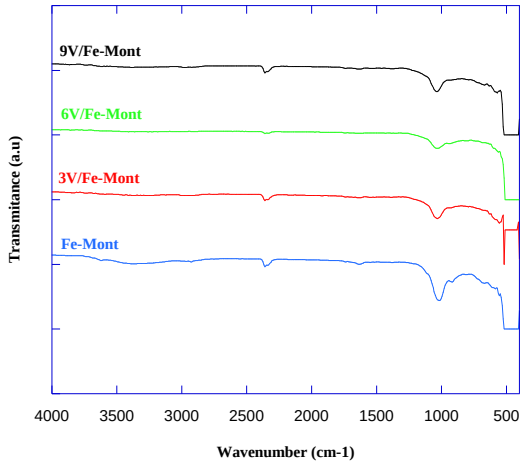

ISSN: 0975-8585

The band around 1600 cm^{-1} is assigned to the bending vibrations of water, and that at around 1060 cm^{-1} corresponds to the asymmetric stretching vibrations of SiO_2 in the tetrahedral structure [55]. The band at 795 cm^{-1}, together with those at 520 and 470 cm^{-1}, can be ascribed to the Si–O bending vibrations in all the samples. After doping the Fe-Mont with vanadia, the FTIR peak positions remained almost the same. However, at a higher vanadia loading of 9 wt%, a new band is observed at around 820 cm^{-1}, which is assigned to the V-O stretching vibrations arising from the formation of crystalline vanadia species [51, 56, 57].

Figure 4: Infrared spectra of pyridine adsorbed on 6wt. %V/Fe-Mont at different temperatures during thermal treatment

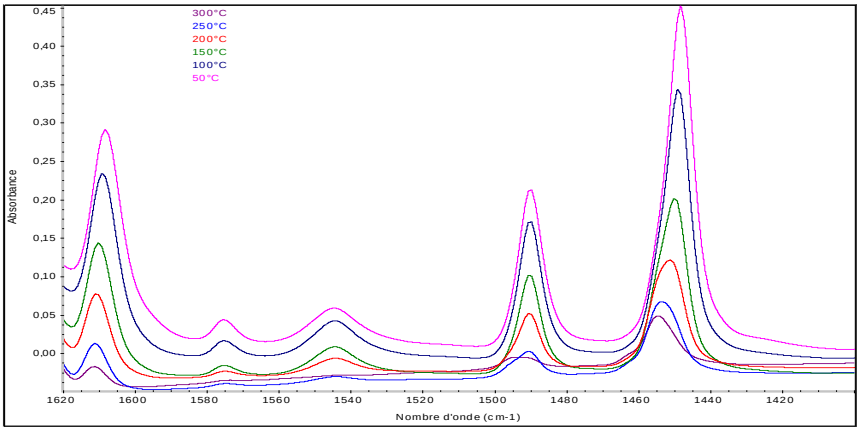

Surface Acidity

The IR-spectroscopy of pyridine adsorption was performed on the surface of all catalysts. The bands of Brønsted acid sites (1538 cm^{-1}) and Lewis acid sites (1448 cm^{-1}) are characteristic of pyridine adsorption on the catalyst surface [58]. Acid sites measured by the spectrophotometric method (Table 1) show that Lewis acidity was highest for the Fe-Mont sample, due to the formation of oxide pillars [59]. However, after doping the Fe-Mont with vanadia, a decrease in Lewis acidity was noted. This decrease is due to the covering of these sites by the increasing amount of V in the catalyst. So the total acidity was found to decrease at higher loadings [60]. This is explained by the stacking of the vanadyl species at the surface of the catalysts; this results in a decrease in the number of adsorption sites exposed.

Table 1: Lewis and Brønsted acid sites estimated by ft-ir spectroscopy

Samples	Number of Lewis acid sites (μ mole g^{-1})	Number of Brønsted acid sites (μ mole g^{-1})
Fe-Mont	404	26
3V/Fe-Mont	302	57
6V/Fe-Mont	165	18
9V/Fe-Mont	141	19

Surface area and pore volume measurements

Surface areas of pillared clays are typically obtained by applying the BET equation to the N_2 adsorption isotherms. Hence, in the present study, the BET surface areas of various systems obtained directly are tabulated. The surface areas of iron-pillared systems are given in table 2. It is noted that the surface area decreases with vanadia doped Fe-Mont because vanadia block the pores of Fe-Mont. The pore volume increases, but at a higher vanadia loading of 9 wt %, a pore volume decrease is observed. The complete adsorption–desorption isotherms of both samples are presented in Fig. 5. All the curves are nearly similar and can be included in type IV in the BDDT classification [61]. The hysteresis loops at low pressure (Fig. 5) indicate

the presence of mesopores [62]. Assuming the pores to be cylindrical, their average radius may be calculated using the formula $r = 2\ V_P / S_p$, where r is the average pore radius, V_p is the pore volume, and S_p is the specific internal surface area of the pores. The average pore radii calculated by this method are tabulated in Table 2. It is interesting to note that the pore size distribution calculated by the BJH equation [63] (Fig.6 and 7) shows the presence of mesopores.

Table 2: Textural properties of vanadia doped iron-pillared clay-based materials

Sample	S_{BET} ($m^2\ g^{-1}$)	V_p ($cm^3\ g^{-1}$)	Ø Pore (nm)
Fe (s)	172	0.21	4.9
3VFe(s)	164	0.24	5.8
6VFe(s)	150	0.25	6.6
9VFe(s)	83	0.17	8.2

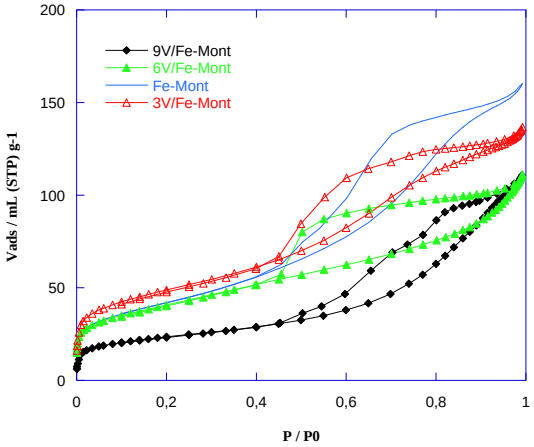

Figure 5:Nitrogen adsorption-desorption isotherms

Figure 6: α-plot of 6V/Fe-Mont.

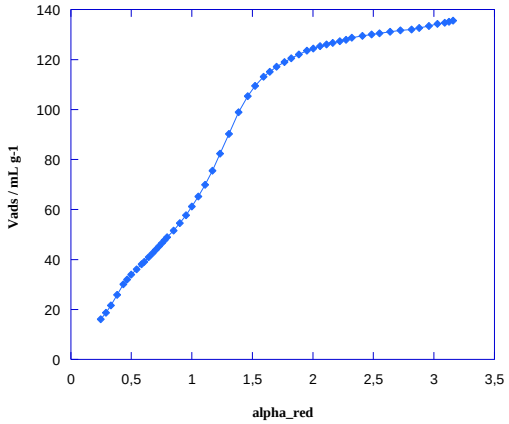

ISSN: 0975-8585

Figure 7: pore size distribution of 6V/Fe-Mont.

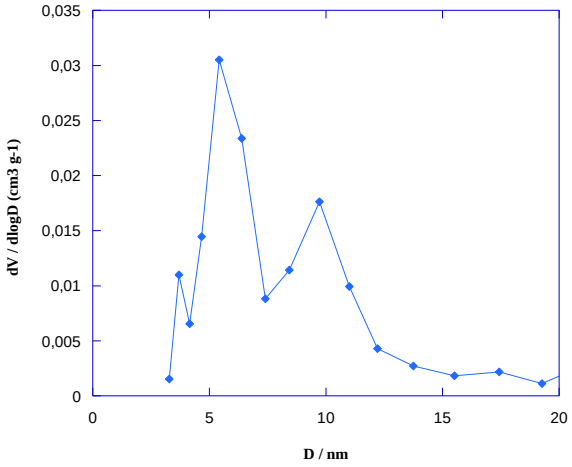

Catalytic test

Optimization of reaction conditions

Reaction conditions were optimized over the clay supported vanadium catalyst. Table 3 shows the plots of vanadium metal wt. % in clay against the conversion and the selectivity to epoxide in the epoxidation of cyclohexene. The cyclohexene conversion reached a maximum value of 87 % for 6 wt.% vanadium-loaded clay and then started decreasing with further increase in vanadium wt.%. As the vanadium wt.% increased beyond 6 %, the excessive vanadium oxide decomposed more TBHP, which is responsible for the decrease of the reactant conversion and the product selectivity [64]. The optimum vanadium content is about 6 %.

The effects of feed ratio on cyclohexene conversion and epoxide selectivity were studied with 1/1, 1.3/1, and 2/1 at 70 C° over 6%V/Fe-Mont for 6 h and the results are given in Table 3. The conversion increased rapidly from 1/1 to 1.3/1 feed ratio, followed by a decrease, while the TBHP concentration increases.Table 3 illustrates also the influence of the oxidant. It is clear that with TBHP there is an epoxidation and with H_2O_2, O_2 there is an allylique oxidation.

Table 3: Cyclohexene oxidation over X wt.%V/Fe-Mont catalysts

Samples	Cyclohexene conversion (%)	TBHP conversion (%)	Selectivity (%)					
			Epoxide	Diol	One	Ol	Enone	Enol
Fe-Mont	20	35	/	/	14	/	/	86
3V/Fe-Mont	46	50	58	/	9	/	13	20
6V/Fe-Mont	87	90	67	7	16	/	7	3
6V/Fe-Mon[a]	58	69	21	14	49	/	11	5
6V/Fe-Mont[b]	46	62	47	7	14	/	4	28
6V/Fe-Mont[c]	11	83	10	/	/	/	55	35
6V/Fe-Mont[d]	59	/	/	/	/	/	100	/
9V/Fe-Mont	50	56	51	/	20	4	13	12

Catalyst = 0.1 g, molar ratio TBHP/Cyclohexene = 1.3, T = 70 °C, t = 6h, solvent n-heptane = 25 mL.
(a), (b) TBHP/Cyclohexene =1, 2, respectively. (c), (d) Oxidant, H_2O_2 and O_2, respectively.

ISSN: 0975-8585

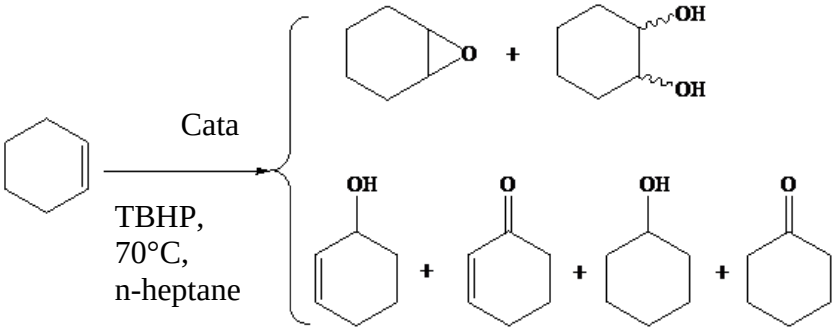

Scheme 1: Products resulting from wcyclohexene epoxidation.

Parameter effects

The amount of catalyst was further optimized by maintaining the reaction temperature at 70 °C. The catalyst amount was increased to 0.2 g under the same reaction conditions. The effect of the catalyst amount is shown in table. 4. The cyclohexene conversion of the substrate reached a peak when the amount of the catalyst was 0.1 g. and then started gradually declining. However, by considering the selectivity to cyclohexene oxide, the catalyst amount of 0.05 g provided the highest cyclohexene oxide selectivity, approximately 71 %, with minimum selectivities to cyclohex-2-en-1-ol and cyclohex-2-en-1-one.

Table 4: Effect of 6%V/Fe-Mont amount on the cyclohexene epoxidation reaction, withTBHP

ass (mg)	Cyclohexene conversion (%)	TBHP conversion (%)	Selectivity (%)					
			Epoxide	Diol	One	Ol	Enone	Enol
0.025	81	81	66	/	18	/	9	8
0.05	72	81	71	/	16	/	7	6
0.1	87	90	67	7	16	/	7	3
0.1[a]	36	40	/	/	7	11	15	67
0.1[b]	21	27	12	/	48	/	/	40
0.1[c]	60	68	82	/	/	/	18	/
0.1[d]	71	75	72	/	/	/	28	/
0.15	75	77	49	25	18	/	4	4
0.2	78	80	50	13	28	/	5	5

Molar ratio TBHP/Cyclohexene = 1.3, T = 70 °C, t = 6h, solvent n-heptane (25 mL).
(a), (b), Solvents, acetonitrile, acetic acid respectively. (c), (d), Temperatures, 50 °C, 60 °C

As shown in Table 4, the solvents also played a critical role in the activity and selectivity in the epoxidation of cyclohexene over V/Fe-Mont. In this study, we investigated the effect of using protic versus aprotic solvents of different polarities (given as dielectric constant). Solvents like heptane (1.9, aprotic), acetonitrile (37, aprotic), and acetic acid (6.2, protic) were investigated; the first number in brackets represents the dielectric strength. It can be seen, from Table 4, that the highest yield in the cyclohexene conversion was recorded in aprotic/apolar solvents, compared to polar solvents, whether protic or aprotic, compared to the recent publication of Farzaneh and his coworkers [65] who obtained contradictory results with H_2O_2 as oxidant. In aprotic solvents, the activity is found to be in this order: acetonitrile < heptane. The product distribution was also significantly influenced by the solvent employed. When heptane was used as solvent, the selectivity to epoxide was the highest, i.e. 65 %, toward epoxide. Although the use of acetonitrile as solvent gave rise to an average cyclohexene conversion (36 %), no epoxide was formed. With acetic acid as solvent, a low cyclohexene conversion (21 %) and selectivity to epoxide (12 %) were observed and a large amount of other products (88 %) was also produced.

The results of cyclohexene conversion and selectivity of products are listed in Table 4, at different reaction temperatures. The temperatures varied from 50 to 70 °C at 1:1.3 molar ratio of cyclohexene/TBHP and 0.1 g of catalyst. It is clear that as the temperature increased, the cyclohexene conversion increased too,

ISSN: 0975-8585

from 68 to 90 %, but the selectivity to cyclohexane epoxide decreased and other products were formed (cyclohexenone, cyclohexanone and alcohols). Subsequently with increasing temperature, more cyclohexane epoxide was oxidized to deep oxidation products and its selectivity decreased.

Energy of activation

The activation energy was calculated using the rate constant (*k*) determined at different temperatures. It is a well-established fact that in the oxidation of hydrocarbons, the rate of the reaction is proportional to the product concentration. The conversion vs time plots obtained in the present work indicate that the cyclohexene oxidation is not an exception to this fact. The reaction is considered to be first order with respect to the product and the reactant concentration. The rate expression for oxidation reactions used by many researchers [37, 66, 67] is adopted here.

$$-\frac{d[cyclohexene]}{dt} = k[cyclohexene] \qquad (1)$$

On integrating expression (1), from the initial concentration at the initial time to the final concentration at the final time *t* , the expression can be written as:

$$-Ln(1-x) = k(t) \qquad (2)$$

X = cyclohexene conversion after time *t.*

A plot of $-Ln(1-x)$ with respect to time gives a linear relationship that shows a pseudo-first-order dependence on cyclohexene, *k* represents the apparent rate constant (Fig. 8a). All the points fall on a straight line; this proves that the rate expression holds good under the conditions employed for the reaction in the present work.

Figure 8(a): First-order kinetic plot for cyclohexene epoxidation by 6 V/Fe-Mont.0.1 g catalyst, TBHP/Cyclohexene molar ratio = 1.3, T = 70 °C, t = 6h, solvent n-heptane (25 mL).

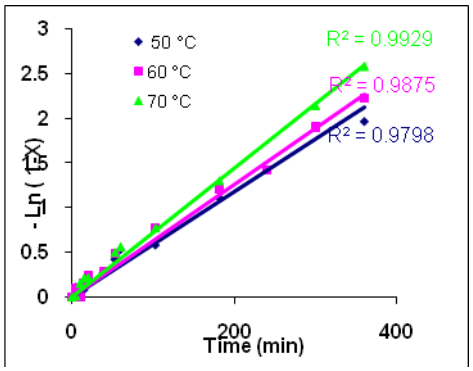

Figure 8(b): displays the graph of $Ln(k)$ obtained from expression (2) for 6 h versus the inverse of the reaction temperature, for each temperature. The apparent activation energy (E_a) calculated from the Arrhenius plot (Fig. 8 b) was ca. 2.114 kcal mol^{-1}. K. C. Gupta et al. and M. Abrantes et al. [36, 37] reported the same apparent activation energy. However, this value was lower than those reported in many previous works (Table 5).

ISSN: 0975-8585

Figure 8(b):Ln(apparent rate constant) vs. inverse of reaction temperature (Arrhenius plot of pseudo-first-order kinetics for epoxidation).

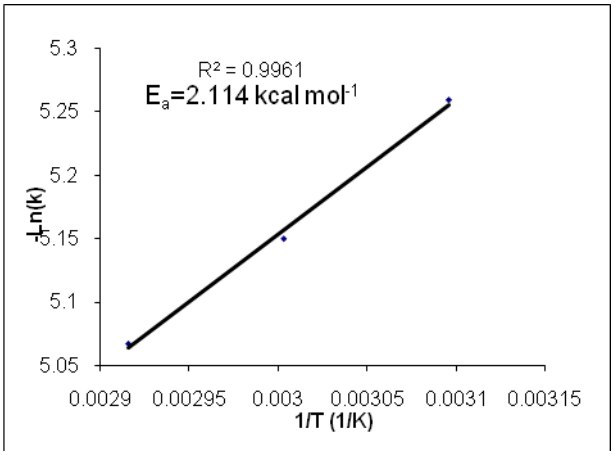

Table 5: E_a determined with different catalysts and different oxidants.

Catalyst	Oxidant	E_a (kcal mol^{-1})	Source
MoO_2(SAL-SH.)DMF	O_2	25.8	[56]
Uncatalysed		20.6	[38]
MnO_2		13.0	[40]
Ru(III)-EDTA	H_2O_2	8.6	[68]
PVMo-Hmont		3.2	[69]
Fe-HPHZ		2.1	[37]
$[(nBu_3Sn)_2MoO_4]$		5.0	[36]
Mo- Cr-α Al_2O_3	TBHP	14.0	[39]
V/Fe-PILC		2.1	Present work

Recycling

The use of heterogeneous catalysts offers several advantages, such as easy recovery and recycling. The recyclability of catalysts for cyclohexene epoxidation with TBHP in n-*heptane* was also tested for two cycles in the optimum reaction conditions previously obtained. From the experimental results, it can be found that the cyclohexene conversion and the selectivity to cyclohexene oxide decreased slightly to 84 and 63 %, respectively. For the second cycle, the results indicated that this material is stable for 2 cycles of reaction. The results of stability of the catalysts 6V/Fe-Mont in the epoxidation reaction of cyclohexene are shown in Table 6 Finally, it can be concluded that at the optimum reaction conditions (70 °C reaction temperature; 0.1 g catalyst; n-heptane; TBHP/cyclohexene ratio, 1.3), within the system under study, 6%V loaded Fe-Mont is a promising catalyst with high catalytic performance for cyclohexene epoxidation with TBHP. Moreover, the recyclability of the catalyst is possible.

CONCLUSION

This work aimed at the preparation of different percentages of vanadium supported on bentonite intercalated with iron in the interlayer space. These materials were essentially characterized by UV-vis diffuse reflectance and FTIR, DRX, BET, and were then tested in cyclohexene epoxidation.

Analysis by UV-Vis diffuse reflection of the catalysts showed the presence of iron and vanadium oxide in the 5+ oxidation state, in monomeric and polymeric forms. FTIR analysis indicated the formation of crystalline vanadium species resulting from the vibration of V-O. Iron intercalated Bentonite showed a low catalytic activity in the epoxidation reaction of cyclohexene, promoting the formation of epoxides. The impregnation of iron intercalated bentonite with vanadium improves the catalytic activity, and promotes the formation of epoxide as the major product, in the presence of heptane as solvent.

Table 6: Results of the stability of 6V/Fe-Mont in the epoxidation reaction of cyclohexene with TBHP.

Cycle	Cyclohexene conversion (%)	TBHP conversion (%)	Epoxide Selectivity (%)
1st	88	89	70
2nd	84	86	63
6 % V/Fe-Mont	87	90	68

0.1 g of catalyst, TBHP/Cyclohexene molar ratio = 1.3, T = 70 °C, t = 6h, solvent n-heptane (25 mL).

The activation energy of catalysts was calculated from the Arrhenius plot which was found to be the lowest compared to what has been reported in the literature.

ACKNOWLEDGMENTS

The authors would like to thank the General Directorate for Scientific Research and Technological Development (DGRST) and Thematic Research Agency for Science and Technology (ATRST) for the financial support to the project PNR-8-U13-880. The authors acknowledge the facilities, and the scientific and technical assistance of LCS, ENSICAEN. They especially thank Mrs. Valérie Ruaux for her help.

REFERENCES

[1] Arfaoui. J, Boudali. L. K and Ghorbel. A, Appl. Clay Sci., 2010, 48, 171-178.
[2] Adams. J. M and McCabe R. W, in Developments in Clay Science, eds. B. K. G. T. Faïza Bergaya and Gerhard. L, Elsevier, 2006, vol. Volume 1, pp. 541-581.
[3] Carriazo. J, Guélou. E, Barrault. J, Tatibouët. J. M, Molina. R and Moreno. S, Catal. Today, 2005, 107-108, 126-132.
[4] Carriazo. J. G, Centeno. M. A, Odriozola J. A, Moreno. S and Molina. R, Appl. Catal. A., 2007, 317, 120-128.
[5] Carriazo. J. G, Martínez. L. M, Odriozola. J. A, Moreno. S, Molina. R and Centeno. M. A, Appl. Catal. B., 2007, 72, 157-165.
[6] Centi. G and Perathoner. S, Micropor.Mesopor. Mater., 2008, 107, 3-15.
[7] De Stefanis. A and Tomlinson. A. A. G, Catal. Today, 2006, 114, 126-141.
[8] Serwicka. E. M and Bahranowski. K, Catal. Today, 2004, 90, 85-92.
[9] Ding. Z, Kloprogge. J. T, Frost. R. L, Lu. G. Q and Zhu. H. Y, J. Pourous. Mater., 2001, 8, 273-293.
[10] Gil. A, Cherkashinin. G. Y and Korili. S. A, Journal of Chemical and Engineering Data, 2004, 49, 639-641.
[11] Gil. A, Korili. S. A and Vicente. M. A, Catal. Rev. Sci. Eng., 2008, 50, 153-221.
[12] Barrera-Vargas. M, Almanza. O. A and Carriazo. J. G, Scientia et Technica, 2007, 35, 489-493.
[13] Kurian. M and Sugunan. S, Microporous and Mesoporous Materials, 2005, 83, 25-34.
[14] Lutz. J. T, Grayson. M, Eckroth. D, Bushey. G. J, Eastman C. I, Klingsberg. A and Spiro. L, Wiley: NewYork, 1980, 9, 251.
[15] Das. D. P and Parida K. M, J. Mol. Catal. A. Chem., 2007, 276, 17-23.
[16] Canali. L and Sherrington. D. C, Chem. Soc. Rev., 1999, 28, 85-93.
[17] De Vos. D. E, Sels. B. F and Jacobs. P. A, Adv. Mater. Catal., 2003, 345, 457-473.
[18] De Vos. D. E., Sels. B. F and Jacobs. P. A, 2001, vol. 46, pp. 1-87.
[19] Jørgensen. K. A, Chem. Rev., 1989, 89, 431-458.
[20] Tang. Q, Wang. C, Hu. S, Sun. H, Chen. Y, Haller. G and Yang. Y, Catal. Lett., 2007, 117, 25-33.
[21] Kaur. N, Singh. B, Kennedy. B. J and Gräfe. M, Geochimica et Cosmochimica Acta, 2009, 73, 582-593.
[22] Gao. X, Bare. S. R, Weckhuysen. B. M and Wachs. I. E, J. Phys. Chem. .B, 1998, 102, 10842-10852.
[23] El-Korso. S, Khaldi. I, Bedrane. S, A. Choukchou-Braham, F. Thibault-Starzyk and R. Bachir, J. Mol. Catal. A. Chem., 2014, 394, 89-96.
[24] El-Korso. S, Rekkab. I, Choukchou-Braham. A, Bedrane. S, Pirault-Roy. L and Kappenstein. C, Bull. Mater. Sci., 2012, 35, 1187-1194.
[25] Lahcene. D, Choukchou-Braham. A, Kappenstein. C and Pirault-Roy. L, Journal of Sol-Gel Science and Technology, 2012, 64, 637-642.
[26] Ameur. N, Bedrane. S, Bachir. R and Choukchou-Braham. A, J. Mol. Catal. A. Chem., 2013, 374, 1-6.

[27] Qiu. C.-J, Zhang. Y.-C, Gao. Y and Zhao. J.-Q, Journal of Organometallic Chemistry, 2009, 694, 3418-3424.
[28] Salavati-Niasari. M, Esmaeili. E, Seyghalkar. H and Bazarganipour. M, Inorganica Chimica Acta, 2011, 375, 11-19.
[29] Reddy. A. S, Chen. C.-Y, Chen. C.-C, Chien. S.-H, Lin. C.-J, Lin. K.-H, Chen C.-L and Chang. S.-C, Journal of Molecular Catalysis A: Chemical, 2010, 318, 60-67.
[30] Hirao. T, Chem. Rev., 1997, 97, 2707-2724.
[31] Leus. K, Vandichel. M, Liu. Y.-Y, Muylaert. I, Musschoot. J, Pyl. S, Vrielinck. H, Callens. F, Marin. G. B, Detavernier. C, Wiper. P. V, Khimyak. Y. Z, Waroquier. M, Van Speybroeck. V and Van Der Voort. P, Journal of Catalysis, 2012, 285, 196-207.
[32] Behera. G. C and Parida. K. M, Applied Catalysis A: General, 2013, 464-465, 364-373.
[33] Mikolajska. E, Calvino-Casilda. V and Bañares. M. A, Applied Catalysis A: General, 2012, 421-422, 164-171.
[34] Corma. A and García. H, Chem. Rev., 2002, 102, 3837-3892.
[35] Busch. D. H, Yin. G and Lee. H.-J, Mechanisms in Homogeneous and Heterogeneous Epoxidation Catalysis, 2011, 45, 119.
[36] Abrantes. M, Valente. A, Pillinger. M, Gonçalves. I. S, Rocha. J and Romão. C. C, J. Catal., 2002, 209, 237-244.
[37] Gupta. K and Sutar. A, J. Mol. Catal. A. Chem., 2008, 280, 173-185.
[38] Mahajani. S, Sharma. M and Sridhar. T, Chem. Eng. Sci., 1999, 54, 3967-3976.
[39] Takehira. K, Hayakawa. T and Ishikawa. T, J. Catal., 1980, 66, 267-280.
[40] Neuburg. H, Phillips. M and Graydon. W, J. Catal., 1975, 38, 33-46.
[41] Visuvamithiran. P, Palanichamy. M, Shanthi. K and Murugesan. V, Appl. Catal. A., 2013, 462–463, 31-38.
[42] Rao. S. N, Munshi. K. N and Rao. N. N, J. Mol. Catal. A. Chem., 1999, 145, 203-210.
[43] Pálinkó. I, Lázár. K, Hannus. I and Kirisci. I, Journal of Physics and Chemistry of Solids, 1996, 57, 1067-1072.
[44] Valverde. J. L, Romero. A, Romero. R, García. P. B, Sánchez. M. L and Asencio. I, Clays Clay Min., 2005, 53, 613-621.
[45] Rao. G. R and Mishra B. G, Materials Chemistry and Physics, 2005, 89, 110-115.
[46] Kumar Rana. R and Viswanathan. B, Catal. Lett., 1998, 52, 25-29.
[47] Gopal Mishra. B and Ranga Rao. G, Microporous and Mesoporous Materials, 2004, 70, 43-50.
[48] Iwamoto. M, Furukawa. H, Matsukami. K, Takenaka. T and Kagawa. S, Journal of the American Chemical Society, 1983, 105, 3719-3720.
[49] Morey. M, Davidson. A, Eckert. H and Stucky. G, Chem. Mater., 1996, 8, 486-492.
[50] Held. A and Florczak. P, Catalysis Today, 2009, 142, 329-334.
[51] Bineesh. K. V, Kim. D.-K, Kim. D.-W, Cho. H.-J and Park. D.-W, Energy & Environmental Science, 2010, 3, 302-310.
[52] Mishra. B and Rao. G. R, J. Pourous. Mater., 2003, 10, 93-103.
[53] Binitha. N. N and Sugunan. S, Microporous and Mesoporous Materials, 2006, 93, 82-89.
[54] Xu. X, Pan. Y, Cui. X and Suo. Z, J. Nat. Gas. Chem., 2004, 13, 204-208.
[55] Carriazo. J. G, Moreno-Forero. M, Molina. R. A and Moreno. S, Appl. Clay Sci., 2010, 50, 401-408.
[56] Reddy. B. M, Ganesh. I and Chowdhury. B, Catal. Today, 1999, 49, 115-121.
[57] Shylesh. S and Singh. A. P, J. Catal., 2004, 228, 333-346.
[58] Chakraborty. B and Viswanathan. B, Catal. Today, 1999, 49, 253-260.
[59] Mishra. T, Parida. K and Rao. S, J. Coll. Inter. Sci., 1996, 183, 176-183.
[60] Chary. K. V. R, Praveen Kumar. C, Venkat Ramana Rao. P and Venkat Rao. V, Catal. Commun., 2004, 5, 479-484.
[61] Brunauer. S, Deming. L. S, Deming. W. E and Teller. E, Journal of the American Chemical Society, 1940, 62, 1723-1732.
[62] Innes. W. B, Anal. Chem., 1967, 39, 79A-80A.
[63] Barrett. E. P, Joyner. L. G and Halenda. P. P, Journal of the American Chemical Society, 1951, 73, 373-380.
[64] Gao. X and Xu. J, Applied Clay Science, 2006, 33, 1-6.
[65] Oki. A. R, Xu. Q, Shpeizer. B, Clearfield. A, Qiu. X, Kirumakki. S and Tichy. S, Catalysis Communications, 2007, 8, 950-956.
[66] Jhung. S. H, Lee. J. H, Cheetham. A. K, Ferey. G and Chang. J. S, J. Catal., 2006, 239, 97-104.

[67] Huh. S, Cho. Y, Jun. M.-J, Whang. D and Kim. K, Polyhedron, 1994, 13, 1887-1894.
[68] Khan. M and Shukla. R, J. Mol. Catal., 1990, 58, 405-413.
[69] S. Boudjema, E. Vispe, A. Choukchou-Braham, J.A. Mayoral, R. Bachir, J.M. Fraile, RSC Advances, 2014, DOI: 10.1039/C4RA13604G.